# Recent advances in surface enhanced Raman spectroscopy (SERS): finite difference time domain (FDTD) method for SERS and sensing applications

By: Zheng Zeng, Yiyang Liu, and Jianjun Wei

Z. Zeng, Y. Liu, J. Wei, Recent advances in surface enhanced Raman spectroscopy (SERS): finite difference time domain (FDTD) method for SERS and sensing applications. *Trends in Analytical Chemistry*. **2016**, 75, 162–173. https://doi.org/10.1016/j.trac.2015.06.009



## Abstract:

There have been significant advancements in the field of surface-enhanced Raman spectroscopy (SERS). Despite being an ultra-sensitive analytical technique, challenges, such as how to get a proper match between the SERS substrate and light for better signal enhancement to obtain a stable, sensitive SERS substrate, prevent its widespread applications. Finite-difference time-domain (FDTD) method, a numerical tool for modeling computational electrodynamics, has recently been used to investigate SERS for understanding the underlying physics, and optimally design and fabricate SERS substrates for molecular analysis. In this review, we summarize the trend of using FDTD method in SERS studies by providing an introduction of fundamental principles, the studies of optical responses, electromagnetic (EM) field distribution, enhancement factor (EF) of SERS, the application in design and fabrication of SERS substrates, and SERS for biosensing and environmental analysis. Finally, the critical issues of using inherently approximate FDTD method and future improvement for solving EM problems and SERS applications are discussed.

**Keywords:** Surface-enhanced Raman spectroscopy (SERS) | Finite-difference time-domain (FDTD) method | Modeling computational electrodynamics | Surface plasmon resonance (SPR) | Electromagnetic (EM) enhancement, metallic nanostructure | Nanofabrication | Single molecular analysis | Biosensing

## Article:

### 1. Introduction

The basic concept of surface-enhanced Raman spectroscopy (SERS) is that the Raman scattering signal of molecules at or close to the surface could be enhanced to a factor of $10^{10}$–$10^{11}$ using large local field enhancements at metallic surfaces under the right conditions [1], [2]. SERS has been employed and widely used as a powerful spectroscopic tool for sensitive and specific detection of chemical [3], biological [4], and medical analytes [5]. In particular, it has progressed from studies of model systems on roughened electrodes to highly sophisticated studies, such as

single-molecule spectroscopy due to the amplification of electromagnetic (EM) fields generated by the excitation of localized surface plasmons [6].

Theoretically, there is no real controversy on the issue of EM versus chemical enhancement, although the mechanism of SERS is still a debate in the literature. Chemical enhancement requires chemical and/or EM interactions resulting from some probes with different intrinsic properties when adsorbed on the metal compared to free space. However, even in the absence of the probe, the EM enhancement would present by itself [1], [7]. Therefore, the EM enhancement plays a dominant role since polarization, excitation, and size and shape dependence were found to be qualitatively consistent with the surface plasmon-based theory in SERS studies [5]. In order to determine the EM fields in enhanced spectroscopy and understand more qualitatively and quantitatively the link between the EM and the underlying localized surface plasmon resonances (LSPRs) of the substrate, analytical and numerical tools have been applied to solve the EM problems. One crucial feature of the analytical solutions is that underlying physical concepts are simple to understand. Unfortunately, more details are mathematically challenging, and numerical approaches are the desirable option in many practical cases. With the help of Matlab software and the increasing computing power of PCs, several numerical techniques, such as finite element method (FEM) [8], finite difference time domain (FDTD) [9], discrete dipole approximation (DDA) [10], and multiple multipole (MMP) [11] have been proposed. A few articles reported the comparison of the abovementioned numerical methods for the analysis of plasmonic properties with specific metallic nanostructures [12], [13], [14]. A more comprehensive comparison of these modeling techniques, with respect to the operation, speed, expenses, and accuracy, would be beneficial to readers, which, however, is out of the scope of this review. Among all these methods, FDTD technique has been widely used in SERS, as it includes Maxwell's equations that focus on the EM mechanism [15], shows computational electrodynamics that is an important parameter related to SERS intensity [16], and helps search for better noble metal/semiconductor substrates [17]. A series of recent review articles adequately cover the principles of SERS and its applications [18], [19], [20], [21], [22]. They start with a historical development of SERS, followed by an overview on the different types of substrates developed for SERS, from basic concepts to signal enhancement and specific applications. While the FDTD method has been widely used for current SERS research, there is no such review article that provides an instructive introduction of the modeling method associated with the development of SERS substrates and their applications.

SERS was first reported over 40 years ago, and it has experienced the periods of highs and lows from the fundamental understanding of the phenomenon to the exploration of promising applications. The observation of the SERS spectra from single molecules led to a second wave of studies. It is currently a topic of great interest, with over 1000 papers published per year. This review has included only a few of these studies on the state-of-the art progress in SERS substrates and their applications in the FDTD–SERS field. In this review paper, we firstly provide a brief description of the theory behind the technique. Then, a systematic review is made on the FDTD simulations in SERS calculations by identifying different parameters such as EM field distribution and optical responses. Other issues regarding the method limitations, research challenges, and future trends are also discussed.

## 2. Theory of FDTD

The FDTD method has been widely used to solve Maxwell's equations in complex geometries in the fields of EM and photonics, and it contributes to the simulation of light scattering from metal particles. The basic mathematical and physics formalism behind the FDTD algorithm is discussed as an indispensable background in this section.

## 2.1. Physics basics

Each field component is solved on a discrete spatial and temporal grid cell named Yee Cell proposed in 1966, where an electric component is located on the edges of the box and the magnetic component is positioned on the faces. Moreover, FDTD is a time domain technique with $E(t)$ and $H(t)$. Results collected from the FDTD solver are automatically interpolated to the origin of each grid point. We also want to know the field as a function of wavelength, $E(\lambda)$, or equivalently frequency, $E(\lambda)$ [1].

FDTD method is used to solve Maxwell's equations in nonmagnetic materials:

$$\frac{\partial D}{\partial t} = \nabla \times H \tag{1}$$

$$D(\omega) = \varepsilon_0 \varepsilon_r(\omega) \times E(\omega) \tag{2}$$

$$\frac{\partial H}{\partial t} = -\frac{1}{\mu_0} \nabla \times E \tag{3}$$

where $H$, $E$, and $D$ are the magnetic, electric, and displacement fields, respectively. $\varepsilon$ and $\mu_0$ are the complex relative dielectric constant and magnetic permeability coefficient, respectively.

Furthermore, in three dimensions, Maxwell equations have six EM field components. With the assumption that the structure is infinite in the z dimension and that the fields are independent of z, the Maxwell's equations are split into two independent groups of equations that can be solved in the $x$–$y$ plane only, which results in the transverse electric (TE) and transverse magnetic (TM) equations. Then, we can use the components of $E_x$, $E_y$, and $H_z$ to solve TE equations and those of $H_x$, $H_y$, and $E_z$ to solve TM equations.

$$\frac{\partial E_z}{\partial y} - \frac{\partial E_y}{\partial z} = -\mu_0 \frac{\partial H_x}{\partial t} \tag{4}$$

$$\frac{\partial E_x}{\partial z} - \frac{\partial E_z}{\partial x} = -\mu_0 \frac{\partial H_y}{\partial t} \tag{5}$$

$$\frac{\partial E_y}{\partial x} - \frac{\partial E_x}{\partial y} = -\mu_0 \frac{\partial H_z}{\partial t} \tag{6}$$

$$\frac{\partial H_z}{\partial y} - \frac{\partial H_y}{\partial z} = \varepsilon \frac{\partial E_x}{\partial t} \tag{7}$$

$$\frac{\partial H_x}{\partial z} - \frac{\partial H_z}{\partial x} = \varepsilon \frac{\partial E_y}{\partial t} \tag{8}$$

$$\frac{\partial H_y}{\partial x} - \frac{\partial H_x}{\partial y} = \varepsilon \frac{\partial E_z}{\partial t} \tag{9}$$

Considering that the function *f(x,y,z,t)* denotes the electric or magnetic field in the coordinate system, it can be discretized via the central difference approximation in both space and time:

$$\left.\frac{\partial f(x,y,z,t)}{\partial x}\right|_{x=i\Delta x} \approx \frac{f^n(i+0.5,j,k) - f^n(i-0.5,j,k)}{\Delta x} \tag{10}$$

$$\left.\frac{\partial f(x,y,z,t)}{\partial y}\right|_{y=j\Delta y} \approx \frac{f^n(i,j+0.5,k) - f^n(i,j-0.5,k)}{\Delta y} \tag{11}$$

$$\left.\frac{\partial f(x,y,z,t)}{\partial z}\right|_{z=k\Delta z} \approx \frac{f^n(i,j,k+0.5) - f^n(i,j,k-0.5)}{\Delta z} \tag{12}$$

$$\left.\frac{\partial f(x,y,z,t)}{\partial t}\right|_{t=n\Delta t} \approx \frac{f^{n+0.5}(i,j,k) - f^{n-0.5}(i,j,k)}{\Delta t} \tag{13}$$

Benefiting from the Drude model developed and Fourier transform of the polarization used in the algorithm, FDTD method has been widely applied in SERS simulations [5], [7], [23].

Meanwhile, numerous commercial software have been implemented in the method, as they are simple and convenient to use, and can solve several types of problems. For example, FDTD simulations are used to measure the scattering enhancement of the arbitrarily complex geometries, with a linear simulation, thus making the calculation easier for setup and analysis, and giving broadband results.

The evolution of FDTD technique has progressed from one-dimensional (1D) to three-dimensional (3D), coupled 3D unconditionally stable local 1D FDTD [24], finite-volume time-domain (FVTD) [25], etc. for more stable and less computational time, and to a high-order discontinuous Galerkin time domain (DGTD) which provides an easier way to handle elements of various types and shapes, irregular non-conforming meshes and varying polynomial degree with more flexibility [26], [27]. In addition, a generalized FDTD (G-FDTD) method has been developed for solving the time-dependent linear and nonlinear Schrödinger equation [28].

2.2. Simulation setup

The details of the simulation setup of FDTD method have rarely been mentioned in most of the SERS research, although they are important to clarify EM field distribution, optical response, and enhancement factor simulations. Hence, the main areas of focus and the related guidelines for simulation setup were concluded as follows:

- Define the physical structures: focus on the key part that contributes to SERS, as under proper conditions, both the metallic nanoparticle (MNP) and the plasmonic surface of the substrate can produce LSPR and surface plasmon polariton (SPP). Moreover, the model for the optical constants of noble metals should be close to the real situation.
- Define a simulation region and boundary conditions: set reasonable mesh size and adjust the mesh size first in the reasonable direction. Both reliable result and PC memory should be taken into account. Perfectly matched layer (PML) is used in most cases, while periodic boundary condition (BC) should be used when both the structures and EM fields are periodic.
- Define a source of light: the incident light, a plane wave, usually propagated along the z direction with polarization in the *x*-direction.
- Define monitors to record data for analysis: the middle section of the nanoparticle (NP) layer is often defined by the field monitor.
- Define script commands: for optical response spectrum use.

As an example, Fig. 1 shows a schematic illustration of the FDTD model and additional simulation layout setting details. The spatial distribution of the near-field plasmonic *E*-field for various substrate configurations and AgNP loading densities was performed with a horizontal (*x*) *E*-polarization of the 633-nm excitation under normal incidence. The spatial parameters included a time step of 0.001 fs, a mesh size of 1 nm in all three directions with an orange box indicating the total mesh area, and a background index of 1.0 (air). It should be noted that a very small mesh can lead to large memory requirement and long simulation times. PML BC and periodic BC were applied along *x*-, *y*-, and *z*-boundaries of the unit cell, respectively. The indexes of Ag and substrates followed the data of optical constants of solids [29], [30].

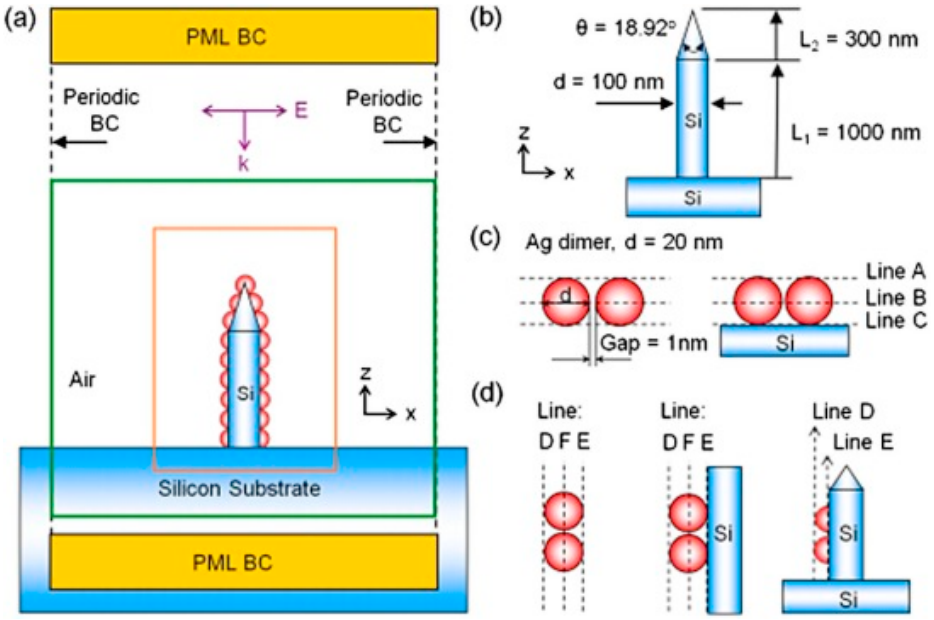


**Fig. 1.** 3D unit cell description and boundary conditions (BC) for FDTD simulation: (a) AgNPs on SiNW; (b) 2.5D NW; (c) horizontal Ag dimer in air, and on bulk Si substrate; (d) vertical Ag dimer in air, on Si substrate, and the AgNP dimer on the 2.5DNW. Lines A–F show position of scan lines along which local *E*-field can be measured and plotted. (Adapted from ref. [30])

## 3. Performance of FDTD method in SERS

From the theoretical description provided earlier, it is evident that the electrodynamic simulations for analyzing SERS can be performed using a number of variables, which results in different FDTD performance for SERS simulation with respect to optical response spectra, EM field distribution, and enhancement factor (EF). In this section, studies that investigate the effect of each performance in SERS are highlighted. In fact, several studies on SERS have been conducted, and this review cannot be exhaustive. Hence, the scope of the SERS field covered in this review article will be limited to recent SERS studies related to FDTD method.

### 3.1. Optical responses

Optical responses including extinction [31], absorption [32], scattering spectra [33], [34], transmittance [35], and reflectance [36], [37] could also be calculated by the FDTD method. The data of optical response versus wavelength are obtained. Among the response parameters, extinction is equal to absorption plus scattering. Table 1 lists the SERS substrates related to optical responses.

**Table 1**. FDTD Applications in Different Kinds of Substrates

| Substrate | Probe | Structure like | Fabrication method | FDTD applications | Enhancement factor | Perspective application | Ref. |
|---|---|---|---|---|---|---|---|
| Ag/Si | R6G | 2.5D NW arrays | Ion-beam sputtering | EM field distribution Absorption peak spectra | ~$3.2 \times 10^6$ | Ultrasensitive toxic screening of food products | [30] |
| GNR/SiNP/CC | DTTC | Ring | Self-assembly | EM field distribution | ~$8.0 \times 10^3$ | Routine chemical/biochemical sensor | [38] |
| Ag/CNAs | R6G | Nanoisland, nanoflowers | Ion-beam sputtering | EM field distribution | ~$5.8 \times 10^7$ | Animal virus biosensing | [39] |
| Ag/$Si_3N_4$ | 4-MP | Nanohole arrays | Nanoimprint lithography | EM field distribution | ~$1.0 \times 10^7$ | Analyte transport and SERS detection | [40] |
| AuNR-AuNP | Thrombin | Protein sandwich | Self-assembly | EM field distribution | ~$1.0 \times 10^7$ | Biomedical applications | [41] |
| Au/$Fe_3O_4$ | R6G | Suspension liquid | Electrostatic interaction | EM field distribution | ~$10^4$–$10^7$ | Practical quantitative detection | [42] |
| Au-Gr-FON | 5'-HS | Nanosphere arrays | Nanosphere lithography | EM field distribution | ~$1.7 \times 10^5$ | Point-of-care HPAIV diagnosis | [43] |
| Au /Si | R6G 4-MP | Nanodot arrays | Template technique; Vapor deposition | EM field distribution | ~$6.5 \times 10^6$ ~$6.8 \times 10^5$ | SERS-related applications | [44] |
| AuNRs | MGITC | SS/EE/ES orientations | Seed-mediated method | EM field distribution | ~$3.0 \times 10^3$-$5.0 \times 10^4$ | Applications for directing anisotropic NPs into well-defined orientations | [45] |
| Ag/SiN | p-ATP | Arrays with nm gap | *E*-beam lithography; Angle evaporation | EM field distribution | ~$1.0 \times 10^9$-$1.0 \times 10^{10}$ | Chemical detection at the single-molecule level | [46] |
| Au-FON | p-ATP | Nanospheres | Self-assembly; Vapor deposition | EM field distribution | ~$1.0 \times 10^6$-$1.0 \times 10^8$ | Plasmonic–photonic microstructures with | [47] |

| Substrate | Probe | Structure like | Fabrication method | FDTD applications | Enhancement factor | Perspective application | Ref. |
|---|---|---|---|---|---|---|---|
| | | | | | | desired spectroscopic functionality | |
| AgNP/AgF/prism | 4-Mpy | Sandwich | Self-assembly | EM field distribution | ~$2.0 \times 10^7$ | A silver nanoparticle-assisted LSP/PSP co-enhanced spectroscopic method | [48] |
| GNSs/Ag or glass | BT | High-density nanostar | Electrostatic interaction | EM field distribution | ~$2.7 \times 10^5$-$4.4 \times 10^7$ | An attomole level of detection of 2,4-dinitrotoluene | [49] |
| Au/Ge | R6G | Ge wafer with Au NPs | Self-assembly | EM field distribution | ~$3.44 \times 10^6$ | Monitoring in situ reaction in an aqueous solution system | [50] |
| Ag | 4-ATP | Nanoplate arrays | Electrodeposition; In situ electrocorrosion | EM field distribution | ~$1.0 \times 10^9$ | DNA hybridization monitoring, protein detection, and virus differentiation | [51] |
| Au@Pd/GC | pyridine | Au-core-Pd-shell NPs | Self-assembly | EM field distribution | ~$5.0 \times 10^4$ | Biological analysis, medical diagnostics, and SM detection | [52] |
| CdSe QDs Au/Si | BT | NP arrays | Self-assembly | Extinction spectra; | ~$1.0 \times 10^4$-~ $1.0 \times 10^8$ | Large NP arrays for SERS applications | [31] |
| HA-MIM | R6G | Hole arrays | Self-assembly | Absorption spectrum; EM field distribution | ~$2.8 \times 10^5$ | Fabrication of arrayed SERS substrate | [32] |
| Au/$SiO_2$ | CNP | Cluster structure | *E*-beam lithography | Scattering spectra | ~$1.0 \times 10^6$ | Applications of SERS interrogated with Fano Resonance | [33] |
| Al/Si | Adenine | Nanovoid | Nanoimprint lithography | Scattering spectra | ~$5.0 \times 10^3$ | Deep-UV SERS applications | [34] |
| Au/Si-ITO glass | 4-MP | Quasi-3D | *E*-beam lithography | Reflectance/transmittance spectra; EM field distribution | ~$1.0 \times 10^9$ | Chemical and biological sensing | [35] |
| AgNP/PATP-SAM/Ag film/prism | p-azo BT | ATR structure | Chemical attachment | Reflectivity spectrum; EM field distribution | ~$2.5 \times 10^9$ | Photochemical dimerization | [36] |
| Au/$SiO_2$-Au-Ti-quartz | 4-ATP | Nanodisk array | *E*-beam lithography | Contour plots of reflectance; EM field distribution | ~$7.8 \times 10^7$ | Biomedical and environmental applications in water | [37] |
| Ag/AAO/PC | R6G | Anemone | Template technique | Enhancement factor | ~$1.0 \times 10^{11}$ | Chemical and plasmonic sensor | [53] |
| Ag/AAO/Al | R6G | Nanostructure arrays | *E*-beam evaporation technique | Enhancement factor | ~$9.77 \times 10^7$ | Detection and characterization of low concentration of molecules | [54] |
| Au/$HfO_2$/graphene | RhB | Sandwich | *E*-beam evaporation | Enhancement factor | ~$6.3 \times 10^5$ | Food safety inspection | [55] |

We could use the FDTD method to obtain optical response spectra in complex structures. For example, Xu et al. used the Fabry–Pérot thin-film model to calculate the reflection coefficients $r_1$ and $r_2$ and the transmission coefficients $t_1$ and $t_2$ of the free-standing hole and the disk layers by FDTD simulations containing only the hole layer or only the disk layer.

Furthermore, the reflection and transmission coefficients, $r$ and $t$, could be obtained for the whole structure, and the reflectance $R$ and transmittance $T$ can be then expressed as $R = r^2$ and $T = t^2$ [35].

It is worth noting that the maximum LSPR wavelength can be determined by the optical response. Modeling of hot spots mentioned earlier was attempted through calculation of the plasmonic near field using the FDTD method. It also required prior calculation of the far-field extinction spectra for the determination of the maximum LSPR wavelength [56]. This wavelength can help determine the part of the SERS substrate contributing to the resonance. The absorption spectrum was simulated to calculate the gap resonance of the proposed hole arrayed metal–insulator–metal (HA–MIM) structure. It showed an absorption peak at the wavelength of 757 nm while no peak for the single gold-layered structure, which revealed that the resonance in the HA–MIM structure was excited by the MIM configuration [32].

FDTD modeling can also be used to verify the experimental optical response. Experimental verification of the scattering spectra was carried out by Ye et al. [33] for each group with carbon (C) NP (CNP) as the Raman-active analyte as it is easily removed by the oxygen plasma [57]. The experimental observations were made based on the self-assembled monolayer (SAM) resulting from thiol–silver or gold bond interactions [58] with the substrate. The reflectivity showed the sharp minimum at 43.6° in air, which is the resonance angle of a propagating surface plasmon (PSP) excitation, and was in good agreement with 43.2° obtained by theoretical evaluation using Fresnel equations as well as FDTD calculations [36]. Besides, the dark-field scattering spectra of the Al nanovoids for deep- ultraviolet (UV) SERS showed the simulated and experimental data. The simulated spectra showed their first-order resonance at 282 nm, which matched well with the experimental data [34]. More importantly, the good consistency between both these data could be applied to verify the accuracy of substrate fabrication. For instance, contour plots of calculated reflectance as functions of different nanodisk pitches in $x$- or $y$-directions and the wavelength were consistent with the experimental results, which indicated that the double-resonance structure had been fabricated as designed with high accuracy [37].

Few studies have been performed to date to investigate the direct effect of optical response on SERS intensity. Most of them focus on the relationship between optical response and electric field. A typical example is the study of the effect of the optical standing waves (SWs) or the leaky mode resonance (LMR) in modulating the total effective $E$-field. In order to address the combined effect of SWs and LMR in a nanowire (NW) system, detailed FDTD calculations were performed on the 2.5D semiconductor nanostructures decorated with AgNPs. The calculated absorption spectrum showed resonant modes and the calculated absorption peak spectral positions for Si; the results show that LMR ensures higher optical absorption and the SWs provide a modulation of the $E$-field, which is the strongest at the node locations of the SWs [30]. Furthermore, Fig. 2 showed the extinction spectra of the aqueous colloid of 80-nm AuNPs, AuNP arrays on indium tin oxide (ITO)-coated glass, and AuNP aggregates on ITO-coated glass. The optical spectra of the arrays are modified by the strong coupling between AuNPs, as confirmed by the FDTD calculations, which showed complex light-field patterns in the NP array at the “blue” (around 550 nm) and the “red” (around 850 nm) regions by incorporating the geometrical details of the NP arrays and the 20-nm ITO/glass substrate [31].

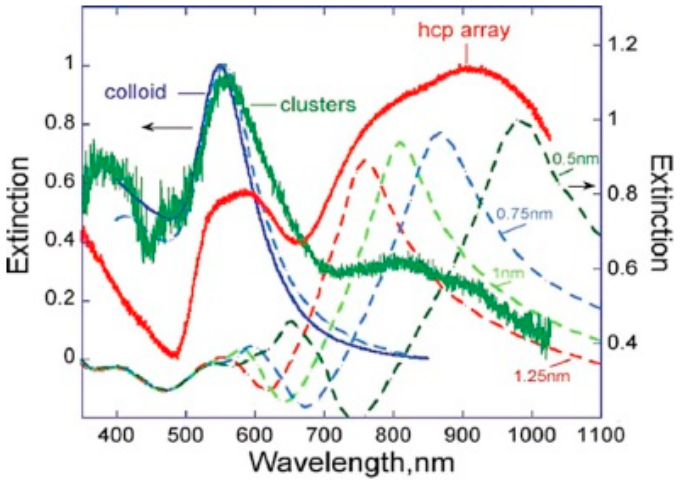


**Fig. 2.** Extinction spectra (normalized by maximum value) of the aqueous colloid of 80-nm AuNPs (blue), AuNP hcp arrays on ITO-coated glass (red), and AuNP aggregates on ITO-coated glass (green). The dashed lines show FDTD calculated spectra of the colloid and ordered NP array with 0.5–1.25 nm gaps. (Adapted from ref. [31])

3.2. Electromagnetic (EM) field distribution

3D-FDTD is an effective tool in simulating the EM field distribution around the illuminated substrate of arbitrary shape by numerical calculation of Maxwell's equations. Several SERS studies have showed the figures of local field distribution [38], electric field distribution [39], electric field intensity [40], and EM near-field enhancement [41] after simulations. In fact, they can be classified as EM field distribution, which is one of the most important FTDT applications in SERS, as shown in Table 1.

The hot spots/active sites of SERS substrates can be confirmed by EM field distribution. The electric field distribution simulations illustrated that the 3D biomimetic SERS substrate provided the hot spot area with high density within a detection volume for enormous SERS enhancement [39]. In addition, the simulations of electric field intensity were performed to demonstrate the increase in the plasmonic field around the nanohole arrays with refractive index-based tuning [40]. Extremely strong EM fields, which contribute to the extraordinarily strong SERS sensitivity, are located across the roughened Ag nanoplate surfaces due to the FDTD simulations. However, in order to accelerate the simulation process, the density of the pits on the simulated model was greatly reduced relative to the experimentally prepared rough Ag nanoplates [51]. By reviewing several studies, an interesting aspect about the hot spots or active sites was observed. The EM field tends to concentrate at the tips of the Au–Gr-coated polystyrene beads where the hot spots formed [43]. According to the electric field distribution in the system containing the prism/silver film/silver NP, the electric field at the gap between the silver film and a silver NP increased by about 4000 times [48]. Farcau and Astilean computed EM field distribution on dimers of Au–HS on top of the polystyrene spheres [47]. For simulation, they found that the enhanced EM fields are located at the junction between the two Au HSs, using a Drude dielectric function for bulk gold and a refractive index of 1.55 for the underlying polystyrene spheres [47]. Hence, the tip, gap, and junction should be focused during SERS research, as strong EM fields are located at these particular sites.

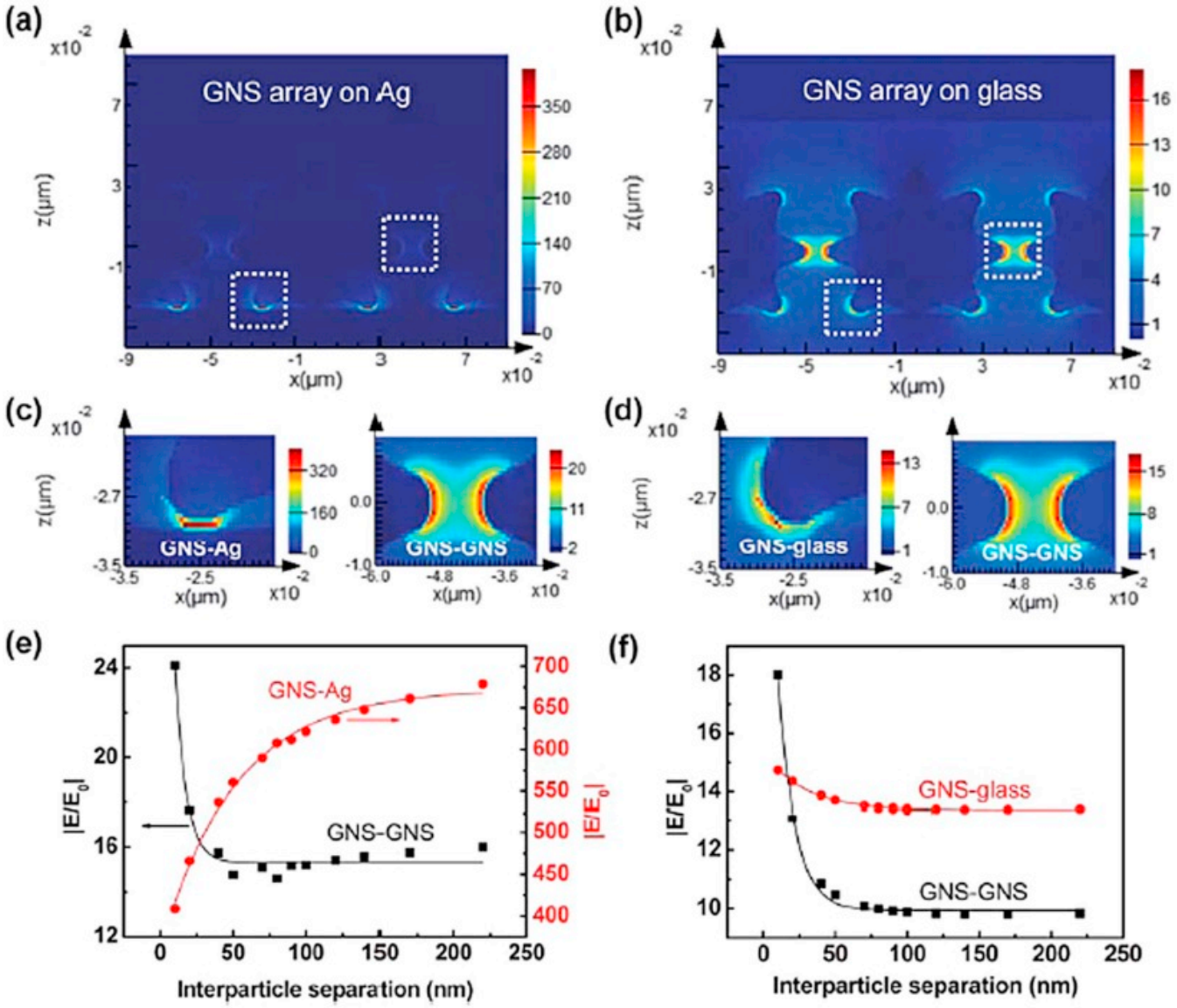


**Fig. 3.** FDTD simulations of E-fields on GNS assemblies on Ag and glass substrates with an inter-particle distance of 10 nm: (a) GNSs on Ag; (b) GNSs on glass; (c) E-fields at the GNS-Ag film gap and the GNS-GNS gap; (d) E-fields at the GNS-glass surface gap and the GNS-GNS gap; (e) local E-field enhancement versus inter-particle separation for (e) GNSs on Ag; (f) GNSs on glass. (Adapted from ref. [52]).

The EM field distribution could be an indicator of the qualities of various kinds of SERS substrates with different inter-particle distances, gap regions, nanopatterns, and fabrication methods. Hu et al. reported the model simulations that demonstrated the effect of the inter-particle distance from 220 to 260 nm on the EM field distribution, although they cannot accurately predict the characteristics of real Au/$Fe_3O_4$ because of the calculation complexity caused by the inhomogeneous and random distribution of the large spheres ($Fe_3O_4$ NPs) and the small ones (AuNPs) [42]. Besides, FDTD simulations were carried out to analyze the EM field distributions for the inter-particle and particle–film gap region, and the SERS EF of gold

nanostars (GNSs) on a metal film as a function of inter-particle separation follows a broken power law function as shown in Fig. 3. The EM field intensities are high in the regions of inter-particle and particle–film gap. Moreover, $[E]/[E_0]$ increases with the increase in inter-particle separation for GNS/Ag, while it increases slightly in the case of GNS/glass [49]. In order to fully understand the electric field distribution of each gold-patterned SERS substrate, and how the 20-nm fold film interacts with gold nanodots, Zheng et al. showed different EM simulations. Besides, they also found that nanopattern geometry had the primary effect on SERS EF over substrate, as, no matter the substrate was covered with gold or not, 55-nm gold dot arrays obtained the strongest EFs [44]. The electric field enhancements of the Au nanorod (AuNRs) assembly motifs in different orientations, side-by-side (SS), end-to-end (EE), and end-to-side (ES), were estimated using the FDTD method. By changing the laser light polarized along the assembled axis to it polarized perpendicularly to the assembled axis, Zhong et al. found that the highest EF in the simulated calculation is taken by the laser light polarized along the assembled axis with the sequence of EE [45].

The EM distribution could also be further applied to confirm EM wave direction and to verify the presence of other effects that contributed to SERS. For example, the local field distribution generated by ring-like assembled gold NRs (GNRs) showed the plane EM wave was polarized along the *x*-axis and propagated along the z-axis [38]. The EM distribution of anodic aluminum oxide (AAO)/Al-based Ag nanostructure arrays was used to demonstrate that the local EM field enhancement and the corresponding SERS are determined by both SPR and interference effects [54]. More importantly, the EF can be roughly calculated from the EM field distribution and has been discussed in section 3.3.

Furthermore, attempts have been made to increase the accuracy of the EM field distribution. The simulation volume needs to be defined and the FDTD simulation parameters could be chosen from the experimental results. For example, the size and shape of AuNRs were taken from the transmission electron microscopy (TEM) statistical data, while the NR orientations were taken into account from the scanning electron microscope (SEM) images [38]. Higher resolution certainly indicates higher computational requirements. A very unique example is the EM response of AgNP pair simulated by defining the spatial extent of the metal NPs from the high-resolution TEM image. FDTD simulations, using a grid of 14 million points to discretize the spatial extent of the electric and magnetic fields with up to 2.5-nm resolution in the gap region and carrying out 200,000 time steps, were performed in multi-teraflop supercomputing facility that consists of 5472 CPUs connected by a high-performance, low-latency Myrinet network [46].

### 3.3. Enhancement factor (EF) simulations

The EF is one of the most important aspect for characterizing the SERS effect and practical applications, as the first concern is generally to know the magnitude of the EF that can be achieved. However, it is difficult to make a single general definition of the EF because of the complex mechanism of EM and chemical enhancement, and the diversity of situations, such as single molecule, multiple molecules, unclear molecule numbers, spatial distribution, and orientations of the probe on the surface [59] This situation will be changed, since a standardization approach has been proposed during the International Conference on Raman Spectroscopy (ICORS) in 2012 in Bangalore, India.

Due to the lack of rigorous definitions, there are three major representative definitions that include the single-molecule EF and the SERS EFs each from the substrate and the analytical chemistry point of view [59] Among these, most studies of SERS EF have indeed focused on the average SERS enhancements across different substrates. The most widely used definition used for the average SERS EF is:

$$\mathrm{EF} = (I_{\mathrm{SERS}}/I_{\mathrm{bulk}})/(N_{\mathrm{ads}}/N_{\mathrm{bulk}})$$

where $I_{\mathrm{SERS}}$ is the Raman signal intensity at a specific vibration mode of the probe molecules attached on the substrate; $I_{\mathrm{bulk}}$ is the normal Raman signal of the probe molecules; and $N_{\mathrm{ads}}$ and $N_{\mathrm{bulk}}$ are the number of probe molecules adsorbed on the substrate and in the bulk exposed to the laser light, respectively. However, as it is difficult to control the number of molecules on each NP and the number of NPs within the focal volume, the number of molecules contributing to an SERS-enhanced signal is generally unknown and is usually ascertained through statistical analysis [46].

We can also use EM field distribution to roughly calculate the EF as mentioned earlier, as the EF is usually defined as ($[E]/[E_0]$) [4] where $E$ is the local maximum electric field and $E_0$ is the input source electric field in a linear simulation [39]. For example, as shown in Fig. 3, the FDTD simulation value of $[E]/[E_0] > 10$ indicated the contribution of EM enhancements to the total EF to be $>10^4$. This method has been widely applied in SERS research. The SERS enhancement [$E$] [4] is about $1.7 \times 10^5$, as the largest local EM field enhancement [$E$] is about 20.5 [43]. Moreover, Theiss et al. reported that the maximum electric field intensity, lying in the gap between the NPs, had a value 82,400 times that of the incident field intensity. Therefore, the SERS enhancement EF, for this NP pair at the most intense point, is given by the square of this electric field intensity EF, giving a value of $6.9 \times 10^9$ [46].

There is a significant relationship between the EF, the excitation wavelength, the analytes, and the composition, size, and geometry of the substrates. The EFs are different based on the association between different parameters, as shown in Table 1. When AuNPs are functionalized at the ends of AuNRs, the enhancement could be increased by 2–3 orders of magnitude, which could significantly improve the signal for target thrombin detection [41]. Besides, the EF values of $10^6$ and $10^8$ were obtained by converting the electric field intensity of $10^3$ and $10^4$ in the case of large and small overlaps, respectively [47]. For a desirable SERS substrate, for example, in the study of metal–dielectric–graphene sandwich for SERS, the EF of $6.3 \times 10^5$ could be obtained by 3D-FDTD simulations, with perfectly matched BC applied in the z-direction while periodic BC set in the $x$- and $y$-directions [55]. The accuracy of substrate fabrication has been ascertained by verifying the EF by the FDTD method. A high EF of $10^{11}$ is ascribed to the significant electric field enhancement at the cavities of nanostructures and nanogaps between them, which is supported by FDTD simulations [53].

## 4. FDTD method for SERS substrate design, fabrication, and its application

Molecules with very low Raman efficiency, samples at very low concentration, and small quantities or volume of samples are the main limitations of the classical Raman spectroscopy.

However, the Raman scattering intensity, arising from molecules located in the vicinity of the nanostructured metallic surface excited by the visible light, can be significantly enhanced because of the excitation of the LSPR [60]. Many probe molecules have been tested [61], and Table 1 shows that Rhodamine 6G (R6G) is the most commonly used probe in SERS. More importantly, SERS is highly dependent upon the substrate. Furthermore, FDTD method has gained much attention for substrate design and fabrication due to the advent of convenient commercial software, which also further promotes the development of SERS techniques.

### 4.1. FDTD method in SERS substrate design and fabrication

In general, there are two main SERS systems. One is the colloid systems that include dispersed optical resonant colloids in solutions, and the other is the substrates with constructing or patterning optical resonant structures [44]. In terms of fabrication method, Sharma et al. presented three representative examples of SERS substrates that include the substrates prepared by bottom-up methods, namely silica-coated clusters of gold NPs, and top-down fabricated immobilized NR assembly (INRA) substrates and tip-enhanced Raman spectroscopy (TERS) tips [20], while Fan et al. classified three general types of substrates, including MNPs immobilized in planar solid supports and metallic nanostructures fabricated using nanolithographic methods and template techniques [19]. Computational modeling tools, such as FDTD, may provide a convenient way for "simulation-based engineering and design optimization" in the SERS substrate fabrication, which enables rapid exploration of multiple design configurations without the need for extensive fabrication and physical testing. The "virtual prototyping" approach for SERS substrate design, rather than conventional trial-and-error-based experimental methods, will benefit the nanofabrication method development and experimental testing in terms of saving fabrication time and cost.

The desirable SERS substrates should possess high SERS sensitivity, good spot-to-spot uniformity (reproducibility and reversibility), and long-term stability of enhanced Raman signals [44]. High SERS sensitivity means large EF. Based on the understanding of the effects of inter-particle gap separation on the particle–film plasmon couplings, Lee et al. fabricated optimally designed SERS substrates with tailored surface plasmons that can detect 2,4-dinitrotoluene on the scale of an attomole [49]. Good spot-to-spot uniformity usually originates from the different areas of a substrate, regardless of geometrical robustness, where there is almost no SERS signal deviation. Lee et al. studied closely spaced gold nanosphere chains on Pt mirrors exhibiting strong plasmon coupling between both horizontally and vertically oriented modes relative to the chain with the FDTD simulation. The broadband enhancement features together with effective light concentration make their structure suitable for the fabrication of reproducible and integrable SERS substrates [62]. Long-term stability requires the long shelf life of high SERS sensitivity. Zheng et al. reported that Raman measurements on an SERS substrate based on large-area well-defined gold NP arrays after 1 year showed almost the same magnitude of Raman signal as that of the original measurement [44].

FDTD method can be used to direct SERS substrate fabrication before experiment, which is a convenient and time-saving compared compared to the trial-and-error approach. In order to match the grating constant of the nanodisk array to excite surface plasmon polaritons (SPPs) in water and to tune the diameter of Au nanodisk for controlling the LSP resonance wavelength,

Shioi et al. first calculated the electric field for a model representing double-resonance substrates, based on Au nanodisk arrays placed in water, by the FDTD method. From the calculation results, they fabricated the desirable double-resonance substrates using electron beam lithography [37]. FDTD calculation was used to explain the size-dependent SERS activity. The SERS-active substrate, being a simple model, was simulated with a fixed inter-particle distance of 2 nm, an excitation laser of 632.8 nm, a Yee cell of $1 \times 1 \times 1$ nm$^3$, and the time steps of 30000. After finding the optimal size, Fang et al. utilized AuNPs as the core to synthesize Au-core-Pd-shell (Au@Pd)NPs to greatly enhance the SERS activity [52]. Furthermore, for the situation that, even with state-of-the-art equipment, high resolution, high crystallinity, and low sidewall roughness cannot be achieved simultaneously, Gao et al. reported that the laser shock imprinting, being a cost-effective direct nanoshaping method, could be used for high-throughput fabrication of smooth 3D crystalline nanostructures at ambient conditions, with FDTD simulations confirming the field enhancement and showing reflectance and absorbance spectra of the simulated structure. Further details are shown in Fig. 4 [63].

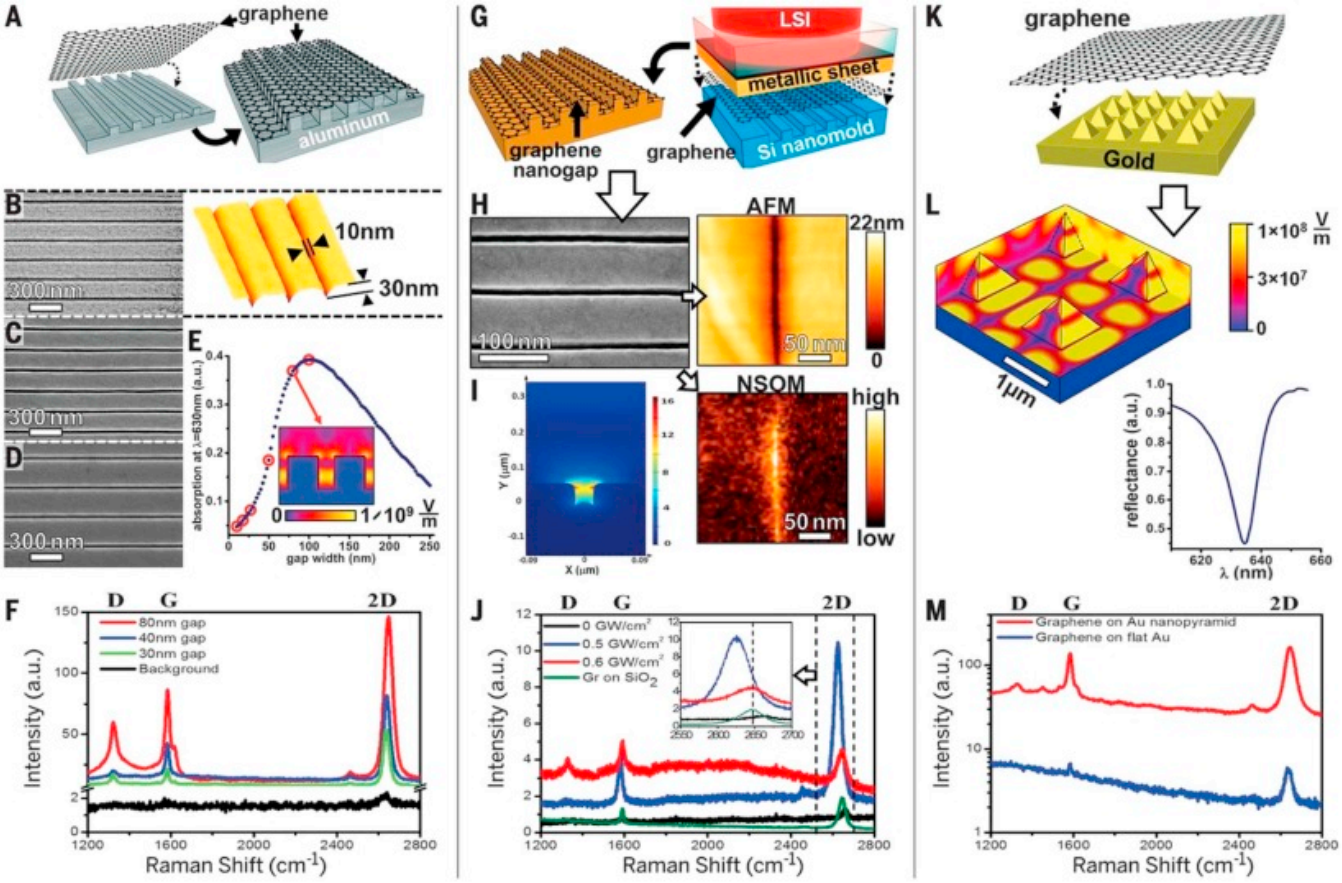


**Fig. 4.** Various ultra-smooth metallic and metal–graphene nanostructures made by laser shock imprinting (LSI) with enhanced EM and optical properties. (A) Schematic image; (B to D) SEM images of periodic aluminum trenches and an AFM image of the Al trench; (E) Absorption spectra; (F) SERS measurement; (G) Schematic image; (H) SEM and AFM images of a graphene–Cu nanogap; (I) FDTD simulation and NSOM measurement; (J) Raman spectrum; (K) Schematic image; (L) FDTD simulations. (M) Raman spectra. (Adapted from ref. [63]).

It is necessary to conclude a discussion of future directions for substrate fabrication. Deep-UV SERS would be highly useful for identifying biological molecules, including protein residues and DNA bases which have electronic resonances in this wavelength range, resulting in both electronic resonance and SERS enhancements. In particular, Al could replace Au and Ag as an alternative plasmonic material for deep-UV SERS, since the strongest enhancements for Au and Ag are found in the visible or near infrared (NIR) region [34]. The promising combination of SERS with spatially offset Raman spectroscopy, that is, SESORS, could contribute to both in vitro on tissue sections and in vivo in small animals in the realm of cancer diagnostics, making it possible to record Raman signals from tissues at depths ranging from millimeter to centimeter, which is a significant step forward in the ability to adapt this approach in a clinical setting for disease diagnosis [21], [64]. The surface-enhanced femtosecond stimulated Raman spectroscopy (SE–FSRS) that combines plasmonics and ultrafast science not only has enabled the study of molecule–plasmon coupling and dynamics, but also can facilitate time-resolved studies of molecular dynamics occurring on or near plasmonic substrates [20]. Therefore, studies on the applicability of desirable substrates for UV–SERS [34], SERORS [65], and SE–FSRS [66] are necessary.

The versatility and flexibility of the FDTD method indicate that it could be used in the study of LSPR, the optical property spectra, and the EF, of different kinds of substrate structures. also In addition, it can also be used investigate the influence of the SERS substrate designed with respect to different material parameters and different structure types, such as the material's refractive index, size, and the shape of the nanostructures, on the position of the LSPR in comparison with the position of the maximum SERS intensity. Thus, the FDTD method could play an important role in the design and the fabrication of substrates.

4.2. The applications of new substrates in analytical science

Currently, SERS has become one of the most sensitive analytical techniques [67], [68], [69], and its applications extend from the investigation of the surface adsorption at the electrode surfaces to analytical studies in the biomedical and environmental areas [19]. Two typical and exciting examples are that three meningitis pathogens were successfully quantified by SERS in a multiplexed test with calculated limits of detection in the picomolar range [70], and Cr(VI) in aqueous solutions was successfully detected using the alizarin red S (ARS)-$TiO_2$ complexes [71]. Furthermore, we conclude some recent typical examples for SERS applications of biosensing and environmental analysis, as shown in Table 2. For example, Wang et al.[78] proposed a kind of quantitative and accurate detection of multiple biomarkers that would allow for the rapid diagnosis and treatment of diseases induced by pathogens with a limit of detection of 1 ng/L.

**Table 2.** Recent Typical SERS Applications for Biosensing and Environmental Analysis

| **Biosensing application** | | | **Environmental analysis** | | |
|---|---|---|---|---|---|
| **Target** | **Limit of detection (LOD)** | **Ref.** | **Target** | **Limit of detection (LOD)** | **Ref.** |
| ATP:ADP molar ratios | 10 nM | [72] | Acetone vapor | 1.7 pg | [73] |
| *Bacillus thuringiensis t-DNA* | 50 pM | [74] | Ametryn | 90 nM | [75] |
| EDC β-estradiol (ESTR) | 300 nM | [76] | Arsenic (As3+) | 0.1 µg/L | [77] |
| Entamoeba histolytica antigen | 58.8 fM | [78] | Azorubine (E122) | 27 mg/L | [79] |
| Genetically modified organisms (GMOs) | 34 fM | [80] | Benzo[a]pyrene (BaP) | 2 nM | [81] |

| Biosensing application | | | Environmental analysis | | |
|---|---|---|---|---|---|
| **Target** | **Limit of detection (LOD)** | **Ref.** | **Target** | **Limit of detection (LOD)** | **Ref.** |
| Glucose | 50 pM | [82] | Dibromide monohydrate (DQ) | 5 nM | [83] |
| H1 Influenza protein | 10 pM | [84] | Ethanol vapor | 3.7 pg | [73] |
| Methylated DNA | 3 pM | [85] | Formaldehyde | 0.17 µg/L | [86] |
| Naphthoic acid (NAPH) | 3.0 µM | [76] | Iodine | 0.2 nM | [87] |
| Nucleic acid | 0.1 nM | [88] | Lead (Pb2+) | 7 nM | [89] |
| K-ras gene | 1.4 pM | [90] | Mercury (Hg2+) | 0.1 µg/L | [91] |
| Potassium hydrogen phthalate (PHTH) | 10 µM | [76] | Metronidazole (MNZ) | 10 µg/L | [92] |
| RNA genetic marker in HPAI virus | 2.67 aM | [43] | Organochlorine pesticides | 10 nM | [93] |
| Sialic acid Organochlorine pesticides | 2 fM | [94] | Polycyclic aromatic hydrocarbons (PAHs) | 6.7 nM | [95] |
| Thrombin | 2.3 fM | [96] | Polybrominated diphenyl ethers (PBDEs) | 2.6 nM | [95] |
| Trypsin | 85 fM | [97] | Polychlorinated biphenyls (PCBs) | 5.3 nM | [95] |
| Vascular endothelial growth factor (VEGF) | 22.6 aM | [98] | Ronidazole (RNZ) | 1 mg/L | [92] |
| Vitellogenin | 5 ng/L | [99] | Tetrabromodiphenyl ether (BDE-47) | 75 nM | [100] |

As shown in Table 1, Table 2 of this review, based on the new substrates associated with FDTD method, SERS could be applied for single-molecule detection, biomedical diagnostic and target detection, environmental analysis, and food safety screening. It has become a sensitive and specific tool due to label-free detection of molecules at very low concentrations and identification of molecules based on their vibrational fingerprints [101].

Arrays of plasmonic NPs with separations on the order of 1 nm could be used in devices used for chemical detection at the single-molecule level, with FDTD simulations predicting an EM SERS EF of $10^9$–$10^{10}$ [46]. A molecular sentinel (MS) probe-modified metal film over nanosphere (MFON) substrate would be applied for point-of-care high pathogenicity influenza (HPAI) virus detection, with FDTD method showing the hot spots at the tips of the Au–Gr-coated polystyrene beads (PS) [43]. The smart liquid SERS substrates based on $Fe_3O_4$/AuNPs improved the quantitative detection of analytes and might be a significant step in employing SERS for environmental analysis, with FDTD model verifying the combined effect of the quasi-photonic crystal and the Au NPs on the EM field penetration [42]. A Au/$HfO_2$/grapheme sandwich with a high-k dielectric layer could promote the design of SERS devices for food safety inspection, with FDTD calculations determining optimized thickness of Au and $HfO_2$ [55].

Based on the application of FDTD method, we have highlighted some of the potential applications of the new substrates. Furthermore, with the advent of UV–SERS, SERORS, and SE–FSRS techniques in the near future, as shown in the concept graphs in Fig. 5, the applications could be extended to material imaging, deep Raman signal sensing, and probing of chemical reaction dynamics with new SERS-augmented scientific techniques. It is hoped that this could also improve the development of SERS quantitation-driven sensing for quantitative analysis, which is still the biggest challenge in SERS field.

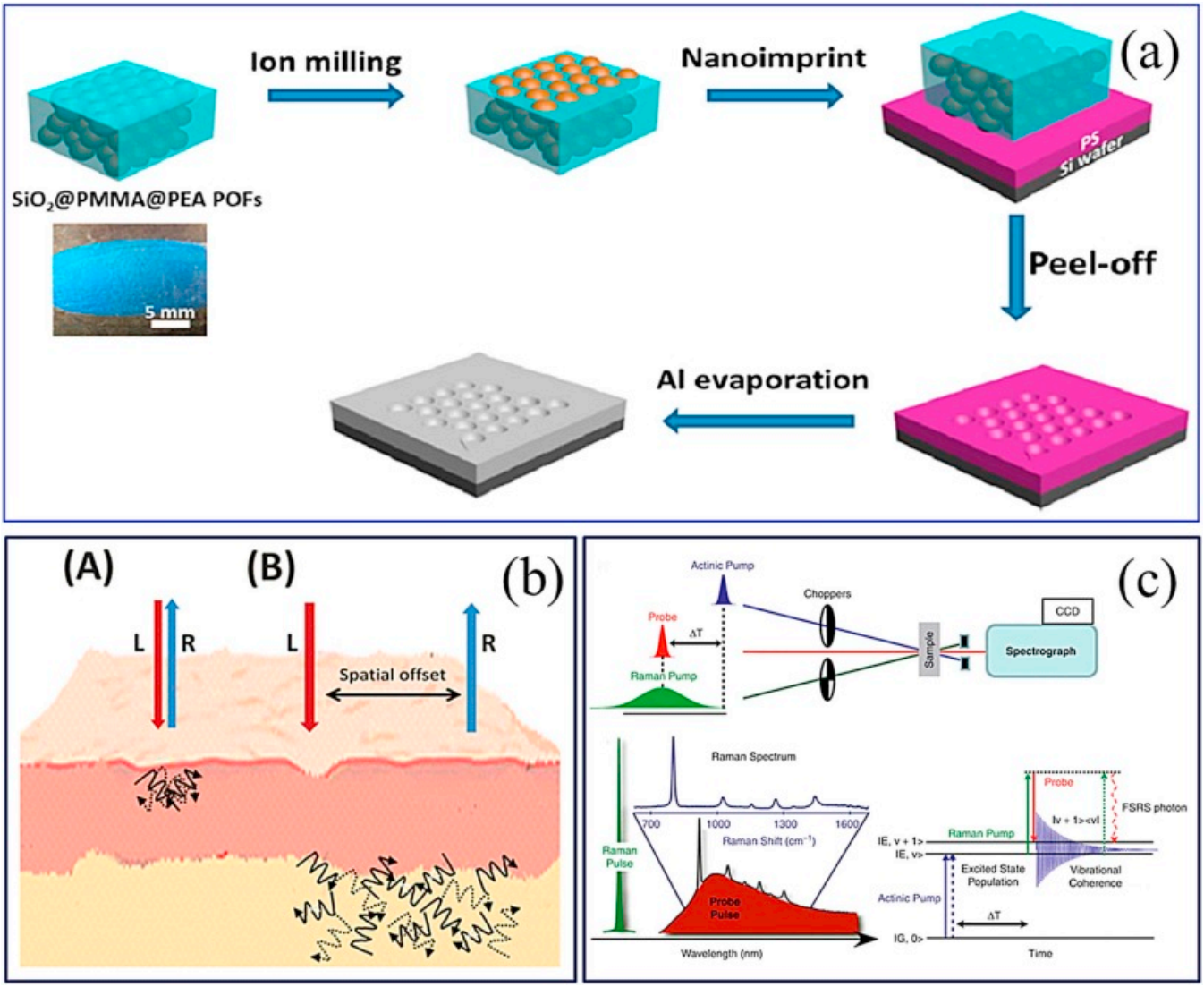


**Fig. 5.** SERS applications are termed UV–SERS, SERORS, and SE–FSRS, respectively: (top a) fabrication procedure of Al nanovoids for UV–SERS; (left b) simplified graphical representation of spontaneous Raman (A) compared to SERORS (B), illustrating the spatial offset and deeper subsurface probing with L = laser light, R = Raman light; (right c) experimental setup for SE–FSRS with Raman spectrum and sketch of mechanism illustration. (Adapted from ref. [[34], [65], [66]].

## 5. Conclusions and outlook

We hope this review can help readers who are interested in both theoretical and experimental studies in the areas of SERS or modeling computational electrodynamics, to better understand the FDTD method in SERS research and sensing applications. FDTD method, being a numerical analysis technique to evaluate Maxwell's differential equations, has become an important tool to calculate the parameters related to SERS intensity. Owing to the versatility and flexibility of the FDTD, it could be used to study the EM field distribution, the optical property spectra, and the EFs of different kinds of substrate structures. It also could be used to indicate the influence of

different parameters and different structure types on SERS intensity, which will further direct SERS substrate design, fabrication, and its applications.

It should also be noted that the FDTD method is inherently approximate; hence, the results obtained from the FDTD method would be approximate regardless of the infinite numeric precision provided by the powerful computers. With this in mind, when we use the FDTD for solving EM problems, for example, the optical response or EM field distribution in SERS substrates, the results can be obtained using a computer if there is no catastrophic failure during the implementation of a solution; however it might not be capable of generating sufficiently accurate results. Fortunately, the development of the improved FDTD method with a finer discretization, such as the abovementioned 3-D FDTD, FVTD, DGTD, and G-FDTD, will give more ways to cross-test the implementation and the solution in EM field, and thus the better results in terms of operation stability, reproducibility, and accuracy. It can be expected that, in the future, FDTD method will be used more often to understand the EM mechanisms, to design and fabricate SERS substrates for high enhancement factor, excellent reproducibility, and long-term stability for highly sensitive, quantitative molecular analysis in real-world applications.

**Acknowledgments**

The authors thank the financial support from the Joint School of Nanoscience and Nanoengineering (JSNN), UNCG for this work.

**References**

[1] E.C. Le Ru, P.G. Etchegoin, Principles of Surface-Enhanced Raman Spectroscopy and Related Plasmonic Effects, first ed., Elsevier, Amsterdam, 2008.

[2] J.P. Camden, J.A. Dieringer, Y.Wang, D.J. Masiello, L.D. Marks, G.C. Schatz, et al., Probing the structure of single-molecule surface-enhanced Raman scattering hot spots, J. Am. Chem. Soc. 130 (2008) 12616‑12617.

[3] S.L. Kleinman, R.R. Frontiera, A.I. Henry, J.A. Dieringer, R.P. Van Duyne, Creating, characterizing, and controlling chemistry with SERS hot spots, Phys. Chem. Chem. Phys. 15 (2013) 21‑36.

[4] L. Guerrini, E. Pazos, C. Penas, M.E. Vazquez, J.L. Mascarenas, R.A. Alvarez-Puebla, Highly sensitive SERS quantification of the oncogenic protein c-jun in cellular extracts, J. Am. Chem. Soc. 135 (2013) 10314‑10317.

[5] Z. Yang, Q. Li, F. Ruan, Z. Li, B. Ren, H. Xu, et al., FDTD for plasmonics: applications in enhanced Raman spectroscopy, Chin. Sci. Bull. 55 (2010) 2635‑2642.

[6] B. Sharma, R.R. Frontiera, A.I. Henry, E. Ringe, R.P. Van Duyne, SERS: materials, applications, and the future, Mater. Today 15 (2012) 16‑25.

[7] S.A. Maier, Plasmonics: Fundamentals and Applications, first ed., Springer US, New York, 2007.

[8] M. Micic, N. Klymyshyn, Y.D. Suh, H.P. Lu, Finite element method simulation of the field distribution for AFM tip-enhanced surface-enhanced Raman scanning microscopy, J. Phys. Chem. B 107 (2003) 1574‑1584.

[9] M. Futamata, Y. Maruyama, M. Ishikawa, Local electric field and scattering cross section of Ag nanoparticles under surface plasmon resonance by finite difference time domain method, J. Phys. Chem. B 107 (2003) 7607‑7617.

[10] M.A. Mahmoud, M.A. El-Sayed, Aggregation of gold nanoframes reduces, rather than enhances, SERS efficiency due to the trade-off of the inter- and intraparticle plasmonic fields, Nano Lett. 9 (2009) 3025‑3031.

[11] M. Hentschel, M. Saliba, R. Vogelgesang, H. Giessen, A.P. Alivisatos, N. Liu, Transition from isolated to collective modes in plasmonic oligomers, Nano Lett. 10 (2010) 2721‑2726.

[12] A. Dhawan, S.J. Norton, M.D. Gerhold, T. Vo-Dinh, Comparison of FDTD numerical computations and analytical multipole expansion method forplasmonics-active nanosphere dimers, Opt. Express 17 (2009) 9688‑9703.

[13] M.A. Yurkin, A.G. Hoekstra, R.S. Brock, J.Q. Lu, Systematic comparison of the discrete dipole approximation and the finite difference time domain method for large dielectric scatterers, Opt. Express 15 (2007) 17902‑17911.

[14] J. Smajic, C. Hafner, L. Raguin, K. Tavzarashvili, M. Mishrikey, Comparison of numerical methods for the analysis of plasmonic structures, J. Comput. Theor. Nanos. 6 (2009) 763‑774.

[15] L. Tong, T. Zhu, Z. Liu, Approaching the electromagnetic mechanism of surface-enhanced Raman scattering: from self-assembled arrays to individual gold nanoparticles, Chem. Soc. Rev. 40 (2011) 1296‑1304.

[16] S.M. Wells, I.A. Merkulov, I.I. Kravchenko, N.V. Lavrik, M.J. Sepaniak, Silicon nanopillars for field-enhanced surface spectroscopy, ACS Nano 6 (2012) 2948‑2959.

[17] T. Wang, Z. Zhang, F. Liao, Q. Cai, Y. Li, S.T. Lee, et al., The Effect of dielectric constants on noble metal/semiconductor SERS Enhancement: FDTD simulation and experiment validation of Ag/Ge and Ag/Si substrates, Sci. Rep. 4 (2014).

[18] P.L. Stiles, J.A. Dieringer, N.C. Shah, R.P. Van Duyne, Surface-enhanced Raman spectroscopy, Annu. Rev. Anal. Chem. 1 (2008) 601‑626.

[19] M. Fan, G.F.S. Andrade, A.G. Brolo, A review on the fabrication of substrates for surface enhanced Raman spectroscopy and their applications in analytical chemistry, Anal. Chim. Acta 693 (2011) 7–25.

[20] B. Sharma, M. Fernanda Cardinal, S.L. Kleinman, N.G. Greeneltch, R.R. Frontiera, M.G. Blaber, et al., High-performance SERS substrates: advances and challenges, MRS Bull. 38 (2013) 615–624.

[21] S. Schlucker, Surface-enhanced raman spectroscopy: concepts and chemical applications, Angew. Chem. Int. Ed. 53 (2014) 4756–4795.

[22] K.A. Stoerzinger, J.Y. Lin, T.W. Odom, Nanoparticle SERS substrates with 3D Raman-active volumes, Chem. Sci. 2 (2011) 1435–1439.

[23] V. Uzayisenga, X.D. Lin, L.M. Li, J.R. Anema, Z.L. Yang, Y.F. Huang, et al., Synthesis, characterization, and 3D-FDTD simulation of Ag@SiO2 nanoparticles for shell-isolated nanoparticle-enhanced Raman spectroscopy, Langmuir 28 (2012) 9140–9146.

[24] I. Ahmed, C. Eng-Kee, L. Er-Ping, C. Zhizhang, Development of the three-dimensional unconditionally stable LOD-FDTD method, IEEE Trans. Antennas. Propag. 56 (2008) 3596–3600.

[25] J.A. Camberos, P.M. Wheat, S.H. Wong, Development and Status of a Finite-Volume, Time-Domain CEM Research Code with Multidisciplinary Applications, Users Group Conference, 2005, pp. 47–51.

[26] H. Fahs, S. Lanteri, A high-order non-conforming discontinuous Galerkin method for time-domain electromagnetics, J. Comput. Appl. Math. 234 (2010) 1088–1096.

[27] S. Dosopoulos, B. Zhao, J.F. Lee, Non-conformal and parallel discontinuous Galerkin time domain method for Maxwell’ s equations: EM analysis of IC packages, J. Comput. Phys. 238 (2013) 48–70.

[28] F.I. Moxley Iii, D.T. Chuss,W. Dai, A generalized finite-difference time-domain scheme for solving nonlinear Schrodinger equations, Comput. Phys. Commun. 184 (2013) 1834–1841.

[29] E.D. Palik, Handbook of Optical Constants of Solids (Book 3), first ed., Academic Press, San Diego, 1997.

[30] Y.F. Huang, C.Y. Chen, L.C. Chen, K.H. Chen, S. Chattopadhyay, Plasmon management in index engineered 2.5D hybrid nanostructures for surface-enhanced Raman scattering, NPG Asia Mater 6 (2014) e123.

[31] A. Chen, A.E. DePrince, A. Demortiere, A. Joshi-Imre, E.V. Shevchenko, S.K. Gray, et al., Self-assembled large au nanoparticle arrays with regular hot spots for SERS, Small 7 (2011) 2365‑2371.

[32] L.P. Xia, Z. Yang, S.Y. Yin, W.R. Guo, J.L. Du, C.L. Du, Hole arrayed metal-insulator-metal structure for surface enhanced Raman scattering by self-assembling polystyrene spheres, Front. Phys. 9 (2014) 64‑68.

[33] J. Ye, F.Wen, H. Sobhani, J.B. Lassiter, P.V. Dorpe, P. Nordlander, et al., Plasmonic nanoclusters: near field properties of the fano resonance interrogated with SERS, Nano Lett. 12 (2012) 1660‑1667.

[34] T. Ding, D.O. Sigle, L.O. Herrmann, D. Wolverson, J.J. Baumberg, Nanoimprint lithography of al nanovoids for deep-UV SERS, ACS Appl. Mater. Interfaces 6 (2014) 17358‑17363.

[35] J. Xu, P. Kvasnicka, M. Idso, R.W. Jordan, H. Gong, J.I. Homola, et al., Understanding the effects of dielectric medium, substrate, and depth on electric fields and SERS of quasi-3D plasmonic nanostructures, Opt. Express 19 (2011) 20493‑20505.

[36] H. Chiba, H. Suzuki, M. Futamata, Highly sensitive Raman spectroscopy using a gap mode plasmon under an attenuated total reflection geometry, Vib. Spectrosc. 73 (2014) 19‑23.

[37] M. Shioi, H. Jans, K. Lodewijks, P. Van Dorpe, L. Lagae, T. Kawamura, Tuning the interaction between propagating and localized surface plasmons for surface enhanced Raman scattering in water for biomedical and environmental applications, Appl. Phys. Lett. 104 (2014) 243102.

[38] V.A. Khanadeev, B.N. Khlebtsov, S.A. Klimova, M.Y. Tsvetkov, V.N. Bagratashvili, G.B. Sukhorukov, et al., Large-scale high-quality 2D silica crystals: dip-drawing formation and decoration with gold nanorods and nanospheres for SERS analysis, Nanotechnology 25 (2014) 405602.

[39] F. Shao, Z. Lu, C. Liu, H. Han, K. Chen,W. Li, et al., Hierarchical nanogaps within bioscaffold arrays as a high-performance SERS substrate for animal virus biosensing, ACS Appl. Mater. Interfaces 6 (2013) 6281‑6289.

[40] S. Kumar, S. Cherukulappurath, T.W. Johnson, S.H. Oh, Millimeter-sized suspended plasmonic nanohole arrays for surface-tension-driven flow-through SERS, Chem. Mater. 26 (2014) 6523‑6530.

[41] Y. Wang, K. Lee, J. Irudayaraj, SERS aptasensor from nanorod-nanoparticle junction for protein detection, Chem. Commun. 46 (2010) 613‑615.

[42] F. Hu, H. Lin, Z. Zhang, F. Liao, M. Shao, Y. Lifshitz, et al., Smart Liquid SERS substrates based on Fe3O4/Au nanoparticles with reversibly tunable enhancement factor for practical quantitative detection, Sci. Rep. 4 (2014).

[43] Y. Pang, J.Wang, R. Xiao, S.Wang, SERS molecular sentinel for the RNA genetic marker of PB1-F2 protein in highly pathogenic avian influenza (HPAI) virus, Biosens. Bioelectron. 61 (2014) 460‑465.

[44] Y. Zheng, W. Wang, Q. Fu, M. Wu, K. Shayan, K.M. Wong, et al., Surface-enhanced Raman scattering (SERS) substrate based on large-area well-defined gold nanoparticle arrays with high SERS uniformity and stability, ChemPlusChem 79 (2014) 1622‑1630.

[45] L. Zhong, X. Zhou, S. Bao, Y. Shi, Y. Wang, S. Hong, et al., Rational design and SERS properties of side-by-side, end-to-end and end-to-side assemblies of Au nanorods, J. Mater. Chem. 21 (2011) 14448‑14455.

[46] J. Theiss, P. Pavaskar, P.M. Echternach, R.E. Muller, S.B. Cronin, Plasmonic nanoparticle arrays with nanometer separation for high-performance SERS substrates, Nano Lett. 10 (2010) 2749‑2754.

[47] C. Farcau, S. Astilean, Mapping the SERS efficiency and hot-spots localization on gold film over nanospheres substrates, J. Phys. Chem. C 114 (2010) 11717‑11722.

[48] Y. Liu, S. Xu, H. Li, X. Jian, W. Xu, Localized and propagating surface plasmon co-enhanced Raman spectroscopy based on evanescent field excitation, Chem. Commun. 47 (2011) 3784‑3786.

[49] J. Lee, B. Hua, S. Park, M. Ha, Y. Lee, Z. Fan, et al., Tailoring surface plasmons of high-density gold nanostar assemblies on metal films for surface-enhanced Raman spectroscopy, Nanoscale 6 (2014) 616‑623.

[50] Z. Zhang, F. Liao, S. Ma, S. Gao, M. Shao, SERS and FDTD simulation of gold nanoparticles grafted on germanium wafer via galvanic displacement, Surf. Interface Anal. 47 (2015) 398‑402.

[51] S. Yang, D. Slotcavage, J.D. Mai, F. Guo, S. Li, Y. Zhao, et al., Electrochemically created highly surface roughened Ag nanoplate arrays for SERS biosensing applications, J. Mater. Chem. C 2 (2014) 8350‑8356.

[52] P.P. Fang, J.F. Li, Z.L. Yang, L.M. Li, B. Ren, Z.Q. Tian, Optimization of SERS activities of gold nanoparticles and gold-core‑palladium-shell nanoparticles by controlling size and shell thickness, J. Raman Spectrosc. 39 (2008) 1679‑1687.

[53] B. Daglar, G.B. Demirel, T. Khudiyev, T. Dogan, O. Tobail, S. Altuntas, et al., Anemone-like nanostructures for non-lithographic, reproducible, large-area, and ultra-sensitive SERS substrates, Nanoscale 6 (2014) 12710‑12717.

[54] D. Shan, L. Huang, X. Li, W. Zhang, J. Wang, L. Cheng, et al., Surface plasmon resonance and interference coenhanced SERS substrate of AAO/Al-based Ag nanostructure arrays, J. Phys. Chem. C 118 (2014) 23930‑23936.

[55] X. Yu, J. Tao, Y. Shen, G. Liang, T. Liu, Y. Zhang, et al., Ametal-dielectric-graphene sandwich for surface enhanced Raman spectroscopy, Nanoscale 6 (2014) 9925‑9929.

[56] A. Sanchez-Iglesias, P. Aldeanueva-Potel, W. Ni, J. Perez-Juste, I. Pastoriza-Santos, R.A. Alvarez-Puebla, et al., Chemical seeded growth of Ag nanoparticle arrays and their application as reproducible SERS substrates, Nano Today 5 (2010) 21‑27.

[57] Z. Zeng, P. Lu, C. Li, L. Mai, Z. Li, Y. Zhang, Removal of NO by carbonaceous materials at room temperature: a review, Catal. Sci. Tech. 2 (2012) 2188‑2199.

[58] J. Wei, H. Liu, A.R. Dick, H. Yamamoto, Y. He, D.H. Waldeck, Direct Wiring of cytochrome c's heme unit to an electrode: electrochemical studies, J. Am. Chem. Soc. 124 (2002) 9591‑9599.

[59] E.C. Le Ru, E. Blackie, M. Meyer, P.G. Etchegoin, Surface enhanced Raman scattering enhancement factors: a comprehensive study, J. Phys. Chem. C 111 (2007) 13794‑13803.

[60] M. Sanders, Y. Lin, J.Wei, T. Bono, R.G. Lindquist, An enhanced LSPR fiber-optic nanoprobe for ultrasensitive detection of protein biomarkers, Biosens. Bioelectron. 61 (2014) 95‑101.

[61] M. Fan, F.J. Lai, H.L. Chou, W.T. Lu, B.J. Hwang, A.G. Brolo, Surface-enhanced Raman scattering (SERS) from Au:Ag bimetallic nanoparticles: the effect of the molecular probe, Chem. Sci. 4 (2013) 509‑515.

[62] Y. Lee, M. Abasaki, A. Portela, J.J. Delaunay, Effective light concentration in gold short nanosphere chain on platinum mirror for surface-enhanced Raman scattering, Appl. Phys. Lett. 105 (2014) 121114.

[63] H. Gao, Y. Hu, Y. Xuan, J. Li, Y. Yang, R.V. Martinez, et al., Large-scale nanoshaping of ultrasmooth 3D crystalline metallic structures, Science 346 (2014) 1352‑1356.

[64] N. Stone, M. Kerssens, G.R. Lloyd, K. Faulds, D. Graham, P. Matousek, Surface enhanced spatially offset Raman spectroscopic (SESORS) imaging ‑ the next dimension, Chem. Sci. 2 (2011) 776‑780.

[65] D.I. Ellis, D.P. Cowcher, L. Ashton, S. O'Hagan, R. Goodacre, Illuminating disease and enlightening biomedicine: Raman spectroscopy as a diagnostic tool, Analyst 138 (2013) 3871‑3884.

[66] J. Dasgupta, R. Frontiera, C. Fang, R. Mathies, Femtosecond Stimulated Raman Spectroscopy, in: G.K. Roberts (Editor), Encyclopedia of Biophysics, Springer, Berlin Heidelberg, 2013, pp. 745‑759.

[67] J.W. Kang, P.T.C. So, R.R. Dasari, D.K. Lim, High resolution live cell raman imaging using subcellular organelle-targeting SERS-sensitive gold nanoparticles with highly narrow intra-nanogap, Nano Lett. 15 (2015) 1766‑1772.

[68] W.D. Li, F. Ding, J. Hu, S.Y. Chou, Three-dimensional cavity nanoantenna coupled plasmonic nanodots for ultrahigh and uniform surface-enhanced Raman scattering over large area, Opt. Express 19 (2011) 3925‑3936.

[69] L.J. Xu, Z.C. Lei, J. Li, C. Zong, C.J. Yang, B. Ren, Label-free surface-enhanced Raman spectroscopy detection of DNA with single-base sensitivity, J. Am. Chem. Soc. 137 (2015) 5149‑5154.

[70] K. Gracie, E. Correa, S. Mabbott, J.A. Dougan, D. Graham, R. Goodacre, et al., Simultaneous detection and quantification of three bacterial meningitis pathogens by SERS, Chem. Sci. 5 (2014) 1030‑1040.

[71] W. Ji, Y. Wang, I. Tanabe, X. Han, B. Zhao, Y. Ozaki, Semiconductor-driven "turn-off" surface-enhanced Raman scattering spectroscopy: application in selective determination of chromium(vi) in water, Chem. Sci. 6 (2015) 342‑348.

[72] H. Fang, H.J. Yin, M.Y. Lv, H.J. Xu, Y.M. Zhao, X. Zhang, et al., Approach for determination of ATP:ADP molar ratio in mixed solution by surface-enhanced Raman scattering, Biosens. Bioelectron. 69 (2015) 71‑76.

[73] C.L.Wong, U.S. Dinish, M.S. Schmidt, M. Olivo, Non-labeling multiplex surface enhanced Raman scattering (SERS) detection of volatile organic compounds (VOCs), Anal. Chim. Acta 844 (2014) 54‑60.

[74] K. Chen, L. Wu, X. Jiang, Z. Lu, H. Han, Target triggered self-assembly of Au nanoparticles for amplified detection of Bacillus thuringiensis transgenic sequence using SERS, Biosens. Bioelectron. 62 (2014) 196‑200.

[75] Y. Chen, Z.P. Chen, J.W. Jin, R.Q. Yu, Quantitative determination of ametryn in river water using surface-enhanced Raman spectroscopy coupled with an advanced chemometric model, Chemometr. Intell. Lab. 142 (2015) 166‑171.

[76] C. Fang, N.M. Bandaru, A.V. Ellis, N.H. Voelcker, Beta-cyclodextrin decorated nanostructured SERS substrates facilitate selective detection of endocrine disruptorchemicals, Biosens. Bioelectron. 42 (2013) 632–639.

[77] L. Ye, G. Wen, J. Dong, Y. Luo, Q. Liu, A. Liang, et al., A simple label-free rhodamine 6G SERS probe for quantitative analysis of trace As3+ in an aptamer-nanosol, RSC Adv. 4 (2014) 32960–32964.

[78] Y. Wang, S. Rauf, Y.S. Grewal, L.J. Spadafora, M.J.A. Shiddiky, G.A. Cangelosi, et al., Duplexmicrofluidic SERS detection of pathogen antigens with nanoyeast single-chain variable fragments, Anal. Chem. 86 (2014) 9930–9938.

[79] V. Peksa, M. Jahn, L. Štolcova, V. Schulz, J. Proška, M. Prochazka, et al., Analysis of azorubine (E 122) in sweet drinks, Anal. Chem. 87 (2015) 2840–2844.

[80] S. Uluok, B. Guven, H. Eksi, Z. Ustundag, U. Tamer, I. Boyaci, Designing multilayered nanoplatforms for SERS-based detection of genetically modified organisms, J. Nanopart. Res. 17 (2015) 1–12.

[81] M. Dribek, E. Rinnert, F. Colas, M.P. Crassous, N. Thioune, C. David, et al., Organometallic nanoprobe to enhance optical response on the polycyclic aromatic hydrocarbon benzo[a]pyrene immunoassay using SERS technology, Environ. Sci. Pollut. Res. Int. (2014) 1–7, doi:10.1007/s11356-014-3384-8.

[82] A. Ceja-Fdez, T. Lopez-Luke, A. Torres-Castro, D.A. Wheeler, J.Z. Zhang, E. De la Rosa, Glucose detection using SERS with multi-branched gold nanostructures in aqueous medium, RSC Adv. 4 (2014) 59233–59241.

[83] R. Gao, N. Choi, S.I. Chang, E.K. Lee, J. Choo, Real-time analysis of diaquat dibromide monohydrate in water with a SERS-based integrated microdroplet sensor, Nanoscale 6 (2014) 8781–8786.

[84] J. Perumal, K.V. Kong, U.S. Dinish, R.M. Bakker, M. Olivo, Design and fabrication of random silver films as substrate for SERS based nano-stress sensing of proteins, RSC Adv. 4 (2014) 12995–13000.

[85] J. Hu, C.Y. Zhang, Single base extension reaction-based surface enhanced Raman spectroscopy for DNA methylation assay, Biosens. Bioelectron. 31 (2012) 451–457.

[86] Z. Zhang, C. Zhao, Y. Ma, G. Li, Rapid analysis of trace volatile formaldehyde in aquatic products by derivatization reaction-based surface enhanced Raman spectroscopy, Analyst 139 (2014) 3614–3621.

[87] Q. Liu, X. Zhang, G. Wen, Y. Luo, A. Liang, Z. Jiang, A sensitive silver nanorod/ reduced graphene oxide SERS analytical platform and its application to quantitative analysis of iodide in solution, Plasmonics 10 (2014) 1‑11.

[88] H.N.Wang, A.M. Fales, T. Vo-Dinh, Plasmonics-based SERS nanobiosensor for homogeneous nucleic acid detection, Nanomedicine 11 (2015) 811‑814.

[89] Q. Liu, Y. Wei, Y. Luo, A. Liang, Z. Jiang, Quantitative analysis of trace Pb(II) by a DNAzyme cracking-rhodamine 6G SERRS probe on AucoreAgshell nanosol substrate, Spectrochim. Acta Mol. Biomol. Spectrosc. 128 (2014) 806‑811.

[90] S. Huang, J. Hu, G. Zhu, C. Zhang, Sensitive detection of point mutation using exponential strand displacement amplification-based surface enhanced Raman spectroscopy, Biosens. Bioelectron. 65 (2015) 191‑197.

[91] P. Ma, F. Liang, Q. Yang, D.Wang, Y. Sun, X.Wang, et al., Highly sensitive SERS probe for mercury(II) using cyclodextrin-protected silver nanoparticles functionalized with methimazole, Microchim. Acta 181 (2014) 975‑981.

[92] C. Han, J. Chen, X. Wu, Y.W. Huang, Y. Zhao, Detection of metronidazole and ronidazole from environmental Samples by surface enhanced Raman spectroscopy, Talanta 128 (2014) 293‑298.

[93] J. Kubackova, G. Fabriciova, P. Miskovsky, D. Jancura, S. Sanchez-Cortes, Sensitive surface-enhanced Raman spectroscopy (SERS) detection of organochlorine pesticides by alkyl dithiol-functionalized metal nanoparticles-induced plasmonic hot spots, Anal. Chem. 87 (2014) 663‑669.

[94] T. Gong, Y. Cui, D. Goh, K.K. Voon, P.P. Shum, G. Humbert, et al., Highly sensitive SERS detection and quantification of sialic acid on single cell using photonic-crystal fiber with gold nanoparticles, Biosens. Bioelectron. 64 (2015) 227‑233.

[95] L. Jing, Y.E. Shi, J. Cui, X. Zhang, J. Zhan, Hydrophobic gold nanostructures via electrochemical deposition for sensitive SERS detection of persistent toxic substances, RSC Adv. 5 (2015) 13443‑13450.

[96] F. Gao, L. Du, D. Tang, Y. Lu, Y. Zhang, L. Zhang, A cascade signal amplification strategy for surface enhanced Raman spectroscopy detection of thrombin based on DNAzyme assistant DNA recycling and rolling circle amplification, Biosens. Bioelectron. 66 (2015) 423‑430.

[97] Z. Wu, Y. Liu, Y. Liu, H. Xiao, A. Shen, X. Zhou, et al., A simple and universal “turn-on” detection platform for proteases based on surface enhanced Raman scattering (SERS), Biosens. Bioelectron. 65 (2015) 375‑381.

[98] S. Zhao, W. Ma, L. Xu, X. Wu, H. Kuang, L. Wang, et al., Ultrasensitive SERS detection of VEGF based on a self-assembled Ag ornamented‐AU pyramid superstructure, Biosens. Bioelectron. 68 (2015) 593‐597.

[99] S.K. Srivastava, A. Shalabney, I. Khalaila, C. Gruner, B. Rauschenbach, I. Abdulhalim, Highly Sensitive SERS Based Nano-Sculptured Thin Film Biosensor for the Detection of Vitellogenin: An Endocrine Disruption Biomarker, Advanced Photonics, Optical Society of America, Barcelona, 2014, p. SeM3C.3.

[100] Z. Sun, J. Du, L. Yan, C. Jing, Rapid detection of 2,2′,4,4′-tetrabromodiphenyl ether (BDE-47) using a portable Au-colloid SERS sensor, J. Raman Spectrosc. 45 (2014) 745‐749.

[101] L. Ramanauskaite, V. Snitka, Surface enhanced Raman spectroscopy of l-alanyl-l-tryptophan dipeptide adsorbed on Si substrate decorated with triangular silver nanoplates, Chem. Phys. Lett. 623 (2015) 46‐50.